



Evaluation of different APC operating strategies considering turbine loading and power dynamics for grid support

Florian Pöschke¹ and Horst Schulte¹

¹Department of Engineering I, Control Engineering, Univ. of Applied Sciences HTW Berlin, Germany

Correspondence: Florian Pöschke (poeschke@htw-berlin.de)

Abstract. This work focuses on the design, implementation, and implications of different operational strategies for wind turbines when providing active power control (APC). APC is a necessary functionality for contributing to the stabilization of the electrical grid. Specifically, two different operational strategies are used as the foundation for a model-based control design that allows the turbine to follow a given power demand. The first relies on keeping a constant rotational speed while varying the generator torque to match the power demand. The second approach varies both, the generator torque and rotational speed of the turbine to yield the desired power output. In the power reduction mode, both operational strategies employ the pitch to maintain the desired rotational speed of the turbine and therefore desired power output. The attainable power dynamics of the two closed-loop systems to varying power demands are analyzed and compared. Reduced-order models formulated as transfer functions and suitable for the integration into an upper-level control design are proposed. It is found that the first strategy involving only the generator torque while keeping a constant rotational speed provides significantly faster power control authority. Further, the resulting fatigue loading in turbulent wind conditions is briefly discussed for the two operational strategies, where constant operational storage is emulated to enable a bidirectional variation of the power output. Without any additional load reducing control loops, the results also suggest that this operational strategy is more favorable with regard to the resulting loading of the turbine structure. The simulation studies are conducted for the 5 MW reference turbine using FAST.

1 Introduction

The provision of ancillary services by wind turbines is an increasingly important functionality for a stable and reliable operation of the electric power system (van Kuik et al., 2016). These ancillary services may comprise features like the reaction to frequency deviations for balancing load variations at different timescales (Margaris et al., 2012; Rebello et al., 2020), or supporting black-start of the power system (Shan et al., 2020; Jain et al., 2020). Effectively, these concepts vary the active and reactive power injection to match the demands of the electric grid, and therefore active power control (APC) on a turbine level is involved. Apart from the benefits of a power tracking for the electrical grid, APC has been reported to possibly enhance wind turbine operation by limiting structural loading (Petrović and Bottasso, 2017), reducing and balancing loads within a wind farm (Kazda et al., 2018; Vali et al., 2019) or increasing the wind farm energy yield (Munters and Meyers, 2018; Frederik et al., 2020).



25 To achieve the desired grid stabilizing functionality, power system studies usually consider the turbine as a variable and adjustable power source (Margaris et al., 2012). For participation in grid stabilization, local control loops may be designed on the turbine level resulting in a variation of the power output depending on the measured states of the electrical grid, see e.g., the droop-based approaches in (Margaris et al., 2012; Van de Vyver et al., 2016; Abouzeid et al., 2019) or the comparison of different approaches in Jain et al. (2020). Moreover, wind turbines may be clustered with other distributed power genera-
30 tors into a virtual power plant aiming for a coordinated response governed by a central control scheme. For the design and implementation of these control loops, however, knowledge about the attainable dynamics of the energy conversion system are necessary (Xin et al., 2013; Björk et al., 2021). As a result, simple models are needed capable of portraying the relevant dynamics emerging from power tracking operation of wind turbines.

On the wind turbine level, APC results in an enlarged operational range that needs to be coped by the wind turbine controller
35 compared to the usual strategy that aims for a maximization of the power output in partial-load region and a limitation of power above rated wind speed (Aho et al., 2016; Pöschke et al., 2020; Jain et al., 2020). The operating trajectory that results in the desired power output, however, is not unique and therefore depends on the choice of the operational scheme encoded in the control strategy. This can be illustrated by considering the generator power given as

$$p(v) = \omega_g(v)T_g(v) \quad , \quad (1)$$

40 where ω_g and T_g are the rotational speed and generator torque, respectively, and v represents the current effective wind speed. From (1), it is apparent that a variation of power output to the demand can be achieved by an adjustment of either the rotational speed, the generator torque, or both. Consequently, there is a need to study the implications of different operating strategies for power tracking with regard to the structural loading and the attainable dynamics seen by the electrical grid. An insightful comparison addressing the loading using two different operational schemes to follow a variable power demand is given by
45 Aho et al. (2016). By additionally proposing reduced order models obtained from the simulation data, this paper aims to feed the discussion on the integration of dynamical turbine models for control design and simulation studies of large-scale power systems. The employed model-based control framework allows to enforce similar turbine dynamics with respect to the wind in both investigated schemes, such that fundamental properties only influenced by the operating strategy and subject to varying power demands may be revealed and discussed.

50 **2 Operating strategies**

For this study, two different operating strategies are chosen and compared. In the first strategy, termed **OS1** in the following, the demanded power is achieved by a variation of the generator torque only while keeping the rotational speed at its nominal value at the current wind speed. Contrarily, in **OS2** the controller enforces a variation of both, the generator torque and rotational speed to meet the power demand. Compared to other strategies involving the limited extraction of rotational energy to support
55 frequency events, the control strategies presented here are conceptualized to enable a permanent operation at the desired power level.



With $\omega_{\text{opt}}(v)$ and $T_{\text{opt}}(v)$ being the optimal (or limited above rated power) rotational speed and generator torque depending on the current effective wind speed v , and p_d is normalized desired power output of the turbine, the two strategies used for turbine operation are formalized as follows

$$\begin{aligned}
 \text{OS1 : } & \begin{cases} p(v) = \omega_{\text{opt}}(v)T_{\text{opt}}(v) & \text{if } p_d = 1 \\ p(v) = \omega_{\text{opt}}(v) \underbrace{p_d T_{\text{opt}}(v)}_{=T(v,p_d)} & \text{if } p_d < 1 \end{cases} \\
 \text{OS2 : } & \begin{cases} p(v) = \omega_{\text{opt}}(v)T_{\text{opt}}(v) & \text{if } p_d = 1 \\ p(v) = \underbrace{\sqrt{p_d}\omega_{\text{opt}}(v)}_{=\omega(v,p_d)} \underbrace{\sqrt{p_d}T_{\text{opt}}(v)}_{=T(v,p_d)} & \text{if } p_d < 1 \text{ and } \sqrt{p_d}\omega_{\text{opt}}(v) \geq \omega_{\min} \\ p(v) = \underbrace{l_\omega(v,p_d)\sqrt{p_d}\omega_{\text{opt}}(v)}_{=\omega(v,p_d)} \underbrace{\frac{\sqrt{p_d}}{l_\omega(v,p_d)}T_{\text{opt}}(v)}_{=T(v,p_d)} & \text{if } p_d < 1 \text{ and } \sqrt{p_d}\omega_{\text{opt}}(v) < \omega_{\min} \end{cases} \quad (2)
 \end{aligned}$$

OS1 employs the generator to produce the desired power by a reduction of the torque directly proportional to the demand p_d . In this strategy, the controller is set to enforce the same rotational speed irrespective of the power output demand p_d by an adjustment of the pitch. Contrarily, in OS2 a reduction of both, the rotational speed and the generator torque setpoints proportional to $\sqrt{p_d}$ are designed also incorporating regulation by pitching. The minimum rotational speed was limited to $\omega_{\min} = 0.75$ (or 9.1 rpm for the 5 MW reference turbine) to avoid hitting the first tower eigenfrequency with the 3P excitation of the rotation; see the Campbell diagram for the reference turbine in Jonkman and Jonkman (2016). To achieve this, the operating point depending factor $l_\omega(v,p_d) = \frac{\omega_{\min}}{\sqrt{p_d}\omega_{\text{opt}}(v)}$ is introduced in (2).

3 Control design

The continuous description of the desired operational strategies encoded in (2) is discretized at 280 operating points each. The steady-state inputs of the wind turbine are derived for the corresponding operating points, and subsequently, a linearization analysis using FAST (Jonkman and Jonkman, 2016) is conducted to capture the rotational dynamics at each point. The linearization points are chosen to represent discrete power output values at $p_d = [1, 0.75, 0.5, 0.25]$ at wind speeds covering a range from $v = [5.5, \dots, 25]$ m/s with a denser distribution of operating points around rated wind speed. The resulting linearization points on the power coefficient surface of the considered turbine for the different operational strategies are illustrated in Fig. 1. The operating strategies share a common operational concept for a power demand of $p_d = 1$ (Fig. 1 and (2)), which represents the nominal operating strategy used in wind turbine control for energy maximization. Fig. 1 shows that the introduction of reduced power modes enlarges the range of possible operating points and consequently dynamics that the controller needs to cope with appropriately.

The identified linear model dynamics gained by the linearization procedure are then interconnected to form an overall nonlinear description in a so-called Takagi-Sugeno structure. The framework is based on the definition of convex membership

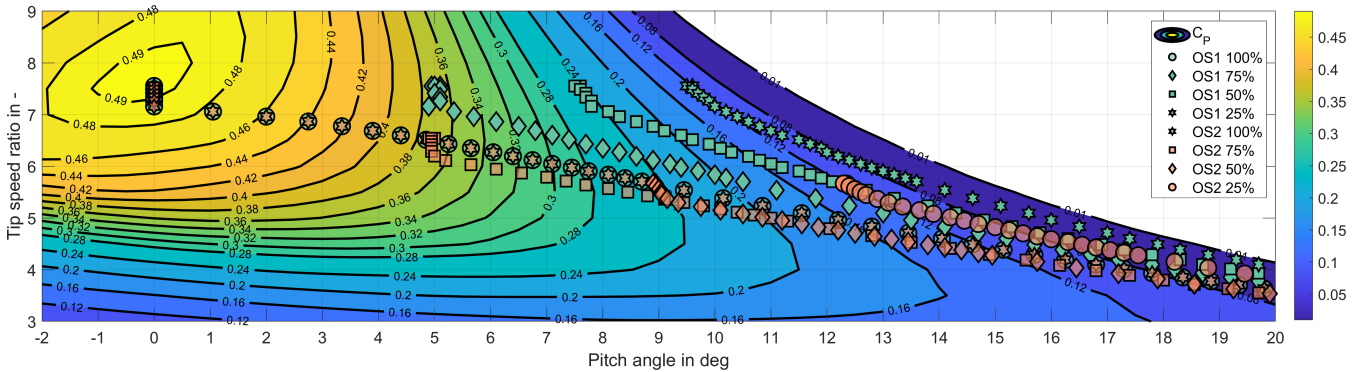


Figure 1. Linearization points on the power coefficient surface for the strategies OS1 & OS2.

functions spanning across the entire operational range, which blend the individual linear submodels in operation depending on the current power output demand, operational strategy, and wind speed.

The control design procedure yields a disturbance observer-based control scheme. Therein, the observer estimates the current effective wind speed by a measurement of the rotational speed. This estimate is used in the calculation of the current operating conditions influencing the membership functions in the nonlinear modeling framework. Further, the estimate determines the calculation of a feedforward term in the control input of the turbine. Details about the applied control scheme and its design process are discussed in (Pöschke et al., 2020). Whereas in (Pöschke et al., 2020) several degrees of freedom including tower or drivetrain dynamics are considered, the applied controller in this work uses the rotational dynamics as only degree of freedom and measured quantity. The control design here follows the lines of the procedure for the rotational dynamics in (Pöschke et al., 2020). It embeds the feedback gain design into a linear matrix inequalities-based optimization problem involving the stability of the closed-loop dynamics. Additional constraints may be introduced to account for performance criteria like decay rates or active damping supplied by the control system in a wide operational range aiming for load reduction at specific turbine components. The model-based design process can be applied to widespread linearization points determined by the control engineer's choice of operational strategy.

Whereas in (Pöschke et al., 2020) OS1 is applied for the simulation studies involving power tracking and load analysis, within this work OS2 is added into the operational spectrum. Effectively, this is achieved by introducing an additional variable as the premise in the Takagi-Sugeno framework used for the nonlinear modeling of the turbine dynamics. This has no effect on the general control approach but introduces an additional dimension in the operating space coped by the premise variables. Even though we present the two operational strategies separately to underline the comparison of resulting loading and power tracking dynamics for the electrical grid, essentially the turbine is operated by one controller that is capable of blending and switching between the different operational strategies.



4 Results

Application of the described control scheme to the FAST (Jonkman and Buhl, 2005) implementation of NREL's 5 MW reference turbine (Jonkman et al., 2009) allows studying the impact of the two operational strategies on the loading and the response time for changes in the power output. The pitch speed is limited to 8 deg/s in all considered scenarios. In the following two sections, the discussed operational strategies are compared from two different perspectives. First, the loading of the turbine structure in some components is briefly analyzed in turbulent wind as this influences the possible choice of operating trajectories with regard to the overall cost of energy. Second, the response time of the power output to instantaneous changes in the power demand is compared for the two operational concepts. Due to the possibly fast dynamics needed in the range of milliseconds to hours (Machowski et al., 2008), the attainable power dynamics of wind turbines is a crucial metric for a successful contribution to grid stabilizing services.

Essentially, the same controller is used for turbine operation in the two strategies. It is capable of blending between the operational strategies as shown in Fig. 2 (a). Therein, it is illustrated how the operational strategy is varied from OS1 at 160 s to OS2 within 15 s, which results in a reduction of the rotational speed until matching the trajectory for the operation of the turbine in OS2 only with the same wind excitation. Subsequently, the opposite change of operational strategy is conducted from 195 s to 210 s. While a small delay in the reduction and increase of rotational speed due to the rotor inertia is visible, the controller is capable of altering the operational strategy online and the turbine trajectories smoothly follow the demand. In Fig. 2 (b) and (c) the resulting generator torque and power output of the turbine are visualized. It can be observed that the two operational strategies OS1 and OS2 result in approximately the same power production, which in this case was set to demand 70% of the available power (or $p_d = 0.7$). When transitioning from OS1 to OS2, an increase of output power is apparent in a time range from 160 s to approx. 175 s, which stems from the energy released due to the decline in rotational speed being previously stored in the turbine rotation. Consequently, the opposite effect is visible when returning to nominal rotational speed by blending from OS2 to OS1 in the time range of 195 s to 210 s.

4.1 Loading in turbulent wind

To compare the structural loading, the turbine was simulated in a turbulent wind field for 40 min, where the power output can be seen in Fig. 2 (d). The wind time series was synthesized using TurbSim (Jonkman and Buhl, 2006) and configuring a normal turbulence model at a mean wind speed of 12 m/s. The rotational speed and power output of the turbine in a time range from 150 s to 260 s are given in Fig. 2 (a) and (c), respectively. The power demand is set to $p_d = 0.7$ to emulate an operational power storage of 30% that can be released into the electrical grid by a variation of the power demand (and of course the opposite way). This flexibility for a reaction to changes in the electrical grid comes at the expense of a 30% reduced energy yield, in this synthesized case.

In Fig. 3 (a), the resulting damage equivalent loads (DELs) of different turbine components are visualized. Therein, the DELs for operational strategy OS2 are normalized to the results when operating the turbine in strategy OS1. An increase in both, tower fore-aft (TwrBsMyt) and tower side-to-side (TwrBsMxt) loading of 14.4% and 21.6% can be observed, respectively.

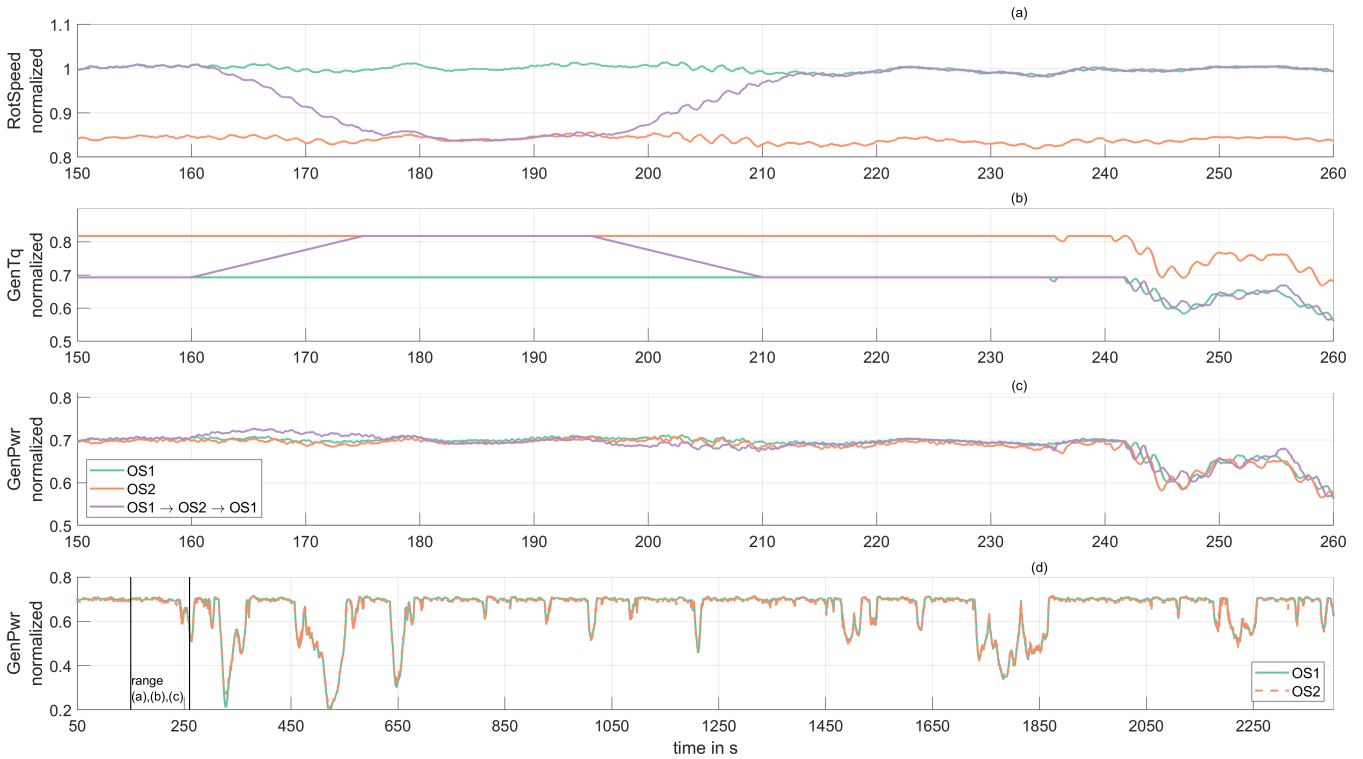


Figure 2. (a) Wind turbine rotational speed, (b) generator torque and (c) turbine power output in turbulent wind for OS1 and OS2 at 70% of power production, where additionally a 15 s ramp transition at 160 s from OS1 to OS2 and back at 195 s is shown. (c) 40 min power output time series in both operational strategies at 70% power production.

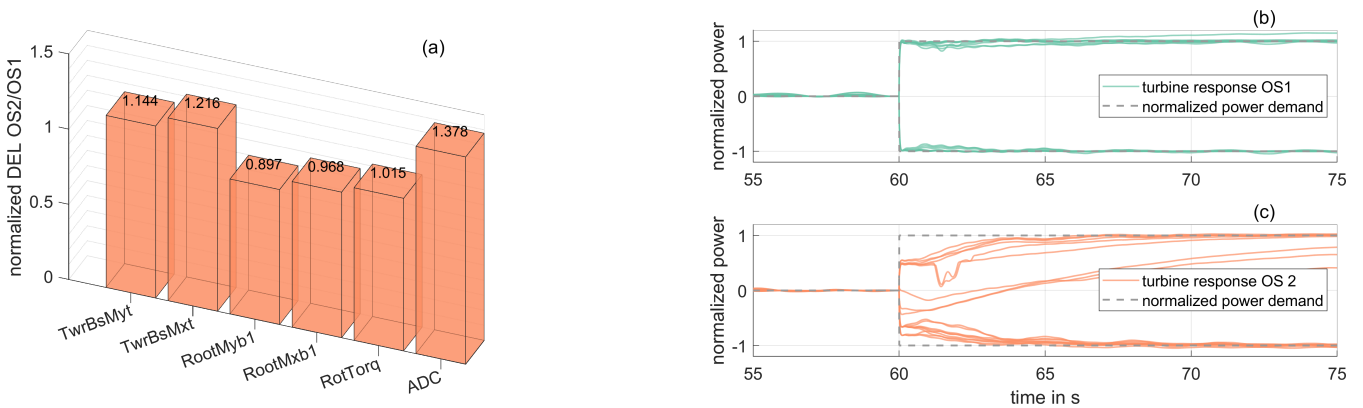


Figure 3. (a) Damage equivalent turbine loads (DEL) of OS2 normalized to OS1 in turbulent wind with mean speed of 12 m/s for 40 minutes. (b&c): Normalized step response for demand steps of $\Delta p_d = \{-0.3, -0.2, -0.1, 0.1, 0.2, 0.3\}$ when operating the turbine at a power reserve with $p_d = 0.7$ in constant wind for (b) in OS1 and (c) in OS2.



135 Contrarily, the blade loading is lower in flapwise (RootMyb1) and edgewise (RootMxb1) direction as characterized by a decline of -10.3% and -3.2% in DEL compared to OS1, respectively. The drivetrain loading, evaluated by the DEL of the rotor torque (RotTorq), suggests only small variations due to different operational strategies, with a moderate increase of 1.5% in OS2 compared to OS1. The pitch activity is greatly affected by the employed operational concept, as can be seen by the 37.8% increase in actuator duty cycle (ADC) (Riboldi, 2016).

140 4.1.1 Discussion: Loading in turbulent wind

Surprisingly, the fatigue loading of the tower is not reduced in OS2, despite of the fewer blade-tower interactions due to the reduced rotational speed, as can be seen in Fig. 3 (a). The simulation results suggest that the greater pitch magnitudes for reacting to the varying wind speed in OS2 compared to OS1, along with the strong coupling of the tower to the pitch movement (Bossanyi, 2003), is responsible for this effect. These results differ from the findings in (Aho et al., 2016), where a reduction in tower loading was predominantly observed in comparable operating scenarios as discussed here. The greater pitch magnitudes
145 needed for balancing the rotational speed to the desired value are also visible in the increased ADC for OS2 shown in Fig. 3 (a), which aligns well with the findings in (Aho et al., 2016). The blade loading is positively affected when operated at a lower rotational speed in OS2 as also reported in (Aho et al., 2016), especially in flapwise direction.

While we have designed a basic controller that only operates based on the rotational speed measurement, the resulting load
150 profiles may be influenced by the introduction of additional performance shaping control architectures. To achieve this, additional degrees of freedom may be introduced into the modeling and design process, yielding feedback loops actively shaping the closed-loop dynamics of components like the drivetrain or the tower movement, as discussed in e.g., (Bossanyi, 2003) or specifically for the applied disturbance observer-based approach used here in (Pöschke et al., 2020). From this perspective, the discussed results within this work constitute a fundamental confrontation of operational strategies without any further load
155 reducing measures. This is supported by our approach to yield similar closed-loop dynamics for both operational strategies by an identical definition of performance constraints formulated in the model-based design process, which results in the similar evolution of the power output that can be seen in Fig. 2 (d).

4.2 Power tracking dynamics

To provide flexible, fast, and predictable control authority to grid stabilizing services and the control loops therein, the response
160 characteristic to changes in the power demand is crucial. To assess the dynamics involved, the turbine is faced with instantaneous demand changes while operating in different constant wind conditions at a constant power output of $p_d = 0.7$. The stepwise changes in the power demand p_d are bidirectional, i.e., increase and reduction of the power output demand at steps of $\Delta p_d = \{-0.3, -0.2, -0.1, 0.1, 0.2, 0.3\}$ is conducted. The simulation is repeated for wind speeds of $v = \{8, 12, 16\}$ m/s roughly covering a range of common operating wind speeds, and in conjunction with the bidirectional steps possibly reveal
165 nonlinear effects. The resulting step responses of the turbine power for operational strategies OS1 and OS2 are depicted in Fig. 3 (b) and (c), respectively. The results therein are normalized to the demanded magnitude for all steps and power production before the event (effectively to result in comparable steps from 0 to 1 or -1).

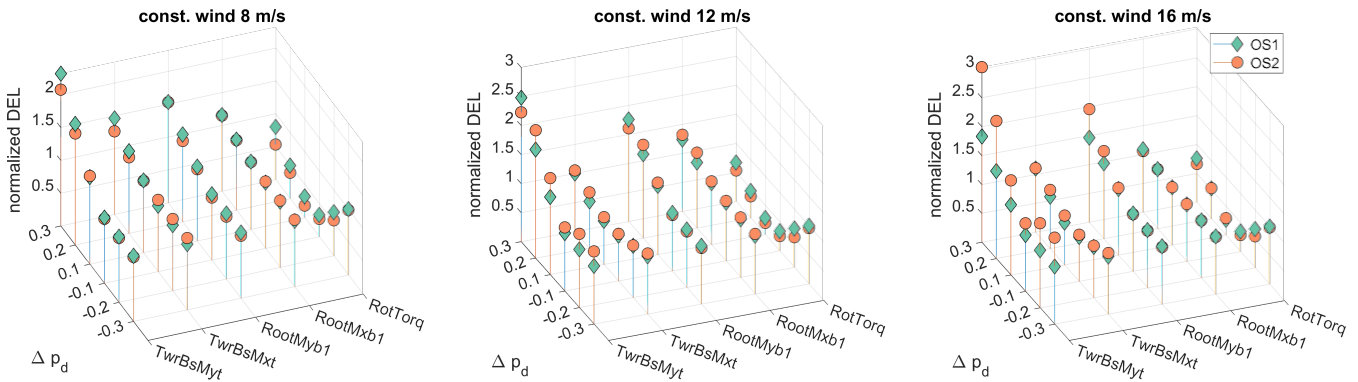


Figure 4. Comparison of normalized ultimate loads for stepwise variation of power demand $\Delta p_d = \{-0.3, -0.2, -0.1, 0.1, 0.2, 0.3\}$ operated in different constant winds. The results are normalized to the ultimate load occurring for a step of $\Delta p_d = -0.3$ in OS1 for each of the considered ultimate load and wind.

Fig. 3 (b) shows that the power output of the turbine precisely follows the demand and is immediately adjusted to the new operating point when operating the turbine in OS1, where only the generator torque and pitch angle are varied for enforcing a constant rotational speed. This holds for both, an increase and decrease of the power demand equally.

In contrast, for OS2 the power output depends on the current operating condition and form of the demand. For a sudden decrease of the power, a settling time of approx. 4 s can be uniformly observed irrespective of the demanded magnitude and current wind speed. However, for an increase in power demand, the power output trajectory is determined by the current inflow conditions. At higher wind speeds, the power output shows similar operating trajectories and settling times as discussed for a power decrease. At lower wind speeds, the settling time rises significantly and also shows a decline at the beginning of the demand step or closely afterwards as can be observed in the trajectories that have not settled to the demanded value at a time of 75 s.

The different operating strategies yield varying amounts of ultimate loading depending on the considered structural turbine component, wind speed and magnitude of the power demand step, which is shown in Fig. 4. The greatest absolute increase in ultimate loading for all considered components is found for a wind speed of 12 m/s, which is an information shadowed by the normalization in Fig. 4. The magnitude of power demand step dictates the additional ultimate loading, where OS1 shows to be superior compared to strategy OS2 in avoiding additional ultimate loading due to the variation of power output especially at greater wind speed (12 m/s and 16 m/s). Contrarily, significant differences in ultimate loading are also found when an increase of power is demanded ($\Delta p_d = \{0.3, 0.2\}$) at low wind speeds, where OS2 shows to be superior to OS1.

185 4.2.1 Discussion & modeling: Power tracking dynamics

The results reveal the dependency of the response characteristic on the employed operational strategy. For OS1, very fast responses to the step demand are possible. This aligns with (Aho et al., 2016), where an increased power tracking performance is found when keeping the rotational speed constant and varying the power with the torque only. The response illustrated in

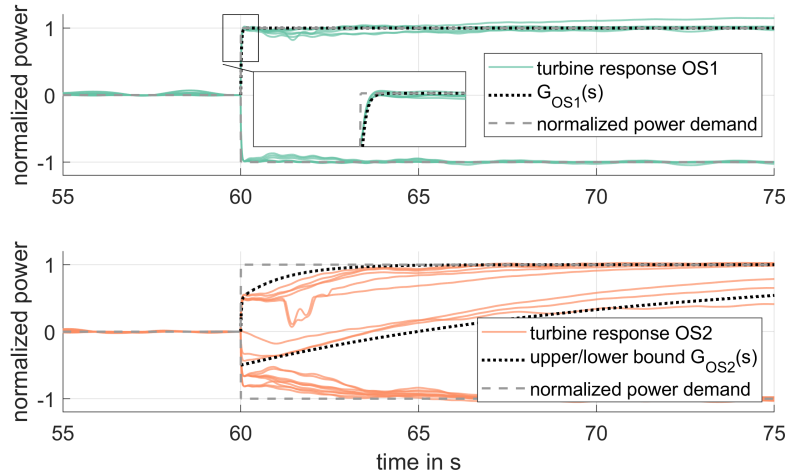


Figure 5. Comparison of step response to the synthetic transfer functions $G_{OS1/OS2}(s)$ designed for control design and simulation studies on a power system level.

Fig. 3 (b) reveals a first-order dynamic behavior in OS1 that can be accounted to the generator torque dynamics used in the simulation model. It is observed that the first-order dynamics is present irrespective of the current wind speed, step magnitude, or direction of step. In the frequency domain, this transfer function can be given as

$$G_{OS1}(s) = \frac{1}{T_{OS1}s + 1} \quad (3)$$

with timescale T_{OS1} governed by the generator torque loop. It is found sufficient for describing the power demand dynamics of the wind turbine if a strategy like (or very similar to) OS1 is chosen by the turbine control engineer. The step response of the transfer function with $T_{OS1} = 20$ m/s is shown in Fig. 5.

If, however, acceleration and deceleration of the turbine is involved in meeting the desired power demand as defined for OS2, the attainable power dynamics depends on the current operating point and direction of the step demand as illustrated in Fig. 4 (c). As a result, an adequate model of the active power dynamics for this strategy depends on the current operating point and step magnitude, revealing the nonlinearities inherited in the system. From Fig. 5 it can be observed that especially an increase in power, i.e., $\Delta p_d > 0$ results in varying response dynamics due to the varying levels of excess power when increasing the power demand¹. Further, it can be observed that the resulting power dynamics is governed by the applied control scheme, which is the cause for the non-minimum phase behavior seen at some operating trajectories. Essentially, this behavior is observed when operating the turbine in partial-load region (i.e., in the simulated cases for a wind speed of $v = 8$ m/s), where the generator torque is employed to control the rotational speed. When the power command increases, the altered rotational speed setpoint results in a reduction of the generator torque by the controller to allow turbine acceleration. This effect necessitates an

¹As the command is normalized to the currently available power, the same magnitude of Δp_d results in different power levels usable for an acceleration of the turbine depending on the wind speed.



extension of the transfer function assigned to OS1 to account for this kind of non-minimum phase behavior that usually is also an important aspect in the modeling of hydro-power for grid studies and control design (Kishor et al., 2007; Björk et al., 2021).

Following the conception of OS2, the response characteristic is governed by two processes consisting of generator torque actuation in parallel to a variation of the rotational speed. The rotation is determined by a combination of excess power for (de-)acceleration and the wind turbine inertia. Following this reasoning, a simple transfer function for OS2 consisting of two parallel paths described as

$$G_{OS2}(s) = G_I(s) + G_{II}(s)$$

with $G_{I/II}(s) = k_{I/II} \frac{a_{I/II}s + b_{I/II}}{c_{I/II}s + d_{I/II}}$ (4)

shows to provide a reasonable match to the simulated turbine step response, see Fig. 5. As the dynamics vary with the wind speed, the transfer function displaying the power dynamics in OS2 needs re-parametrization depending on the current operating point, i.e., the parameters are functions of the wind speed $k/a/b/c/d_{I/II} = f(v)$. The parameters of the "upper" and "lower" bound (for the considered scenarios in Fig. 5) in $G_{OS2}(s)$ are displayed in Tab. 1. While the number of ten parameters might seem complex to parametrize, the two configurations follow a physically interpretable rationale as follows.

Table 1. Values of the transfer functions used for upper and lower bound parametrization in OS2

Parameter	k_I	a_I	b_I	c_I	d_I	k_{II}	a_{II}	b_{II}	c_{II}	d_{II}
Upper bound	0.5	0	1	1.25	1	0.5	0	1	0.02	1
Lower bound	1	0	1	10	1	-1	0.5	0	1	0.05

The upper bound parametrization corresponds to the highest simulated wind speed of $v = 16$ m/s and consists of two parallel first-order functions, i.e., $G_{I/II}(s) = k_{I/II} \frac{1}{c_{I/II}s + 1}$. The two parallel processes consist of torque and rotational speed setpoint variation, and therefore, $c_{I/II}$ describe the dynamics of closed-loop torque and inertia-based rotational speed evolution, respectively. As the concept in OS2 relies on an equal setpoint sharing among torque and rotational speed (established by $\sqrt{p_d}$ in (2)), setting $k_{I/II} = 0.5$ is an intuitive choice. On the other hand, in the lower bound parametrization corresponding to partial-load operation at $v = 8$ m/s, the discussed controller interaction from the rotational speed to the torque actuation plays a dominant role and decays when the desired rotational speed is reached. Therefore, the two parallel process are I: the torque actuated rotation as first-order transfer function $G_I = \frac{1}{c_I s + 1}$ and II: a negative derivative transfer function $G_{II} = -\frac{a_{II}s}{s + d_{II}}$. The influence of $G_{II}(s)$ vanishes as $s \rightarrow 0$ to account for the non-minimum phase behavior stemming from the control interaction. Note that c_I represents the inertia in combination with the available power in both upper and lower bound, but due to the varying power levels substantially depend on the current wind speed, see the parameters in Tab. 1.

From consideration of the ultimate loading, it was found that OS1 by remaining at constant rotational speeds tends to be superior to OS2 in avoiding additional ultimate loading of the components. As concluded for fatigue loading in turbulent wind, the lower pitch magnitudes in OS1 compared to OS2 cause smaller excitation of the turbine structure, and consequently result in lower or similar ultimate loading when instantaneously adjusting the current power demand. Only at the lower wind speed



(8 m/s) and a demanded increase of power, OS2 significantly outperformed OS1 in ultimate loading. Especially those scenarios, however, showed unsatisfactory response dynamics to the power changes in OS2, as discussed for the power output trajectories
235 in Fig. 3 (c). The comparatively low power that is solely available for an acceleration of the turbine has positive effects on the ultimate loading experienced by the turbine in these cases.

5 Conclusions

Within this contribution, it is discussed how different operational strategies can be designed for wind turbines using a model-based control design. The influence on the attainable power dynamics for supporting the electrical grid and the resulting
240 loading are analyzed for synthetically designed scenarios. The presented simulation studies reveal the dependency of the power dynamics on the operational strategy, where it is found that OS1 (keeping the rotational speed constant) provides significantly faster control authority in the power dynamics compared to OS2, where a de- or acceleration of the turbine's rotor is performed. While for OS1 the fast generator dynamics are governing, the response in OS2 is mainly determined by the turbine's inertia. This underlines the additional flexibility in following a power demand in favor of the electrical grid when using OS1, where
245 the amount of injected power can be controlled by the generator torque at a fast scale.

While faster power dynamics in OS1 could be expected, the results from a loading perspective are surprising, which holds for both, the fatigue loading during turbulent wind and the ultimate loading at power demand steps. Except for the decreased blade fatigue loading, it was found that OS1 in the considered turbulent wind scenario and turbine setup showed smaller fatigue loading of the tower despite the greater rotational speed compared to power reduction at OS2. OS1 also tends to decrease the
250 ultimate loads when following a power demand step compared to OS2.

While the presented results suggest an application of OS1 from both considered perspectives, i.e., loading and power dynamics, the considered scenarios within this work are limited, where a variety of different aspects that are not subject of this work can determine the choice of the operational strategy applied to the turbine (also e.g., bird fatalities (Baerwald et al., 2009) or noise emission (Leloudas et al., 2007) decrease with lower rotational speed). It is shown how model-based control
255 introduces flexibility in the choice of operational strategies for wind turbines at comparable dynamical properties. Further, a dedicated control design allows for an online variation of the operational strategy, such that wind turbines can flexibly adjust the operational strategy subject to varying conditions.

For studying stability of the power system with a high share of decentralized generation, the participating power units and their relevant dynamical behavior must be considered and combined with models of the electrical grid. Therefore, modeling
260 approaches are needed capable of portraying relevant dynamical properties, while satisfying complexity constraints to be suitable for the large-scale integration in both advanced control design on a power system level, and the required simulations studies. The results obtained from the simulation studies suggest that the model for portraying the relevant dynamics depends on the chosen operating strategy. When aiming for constant rotational speed in a reduced power mode, a first-order transfer function governed by the closed-loop generator dynamics is seen to provide a reasonable model description. If a simultaneous
265 rotational speed variation is assigned in the control scheme, the inertial response of the turbine rotor in conjunction with the



available excess power needs to be considered in the description. Due to the nonlinearities in the energy conversion process and the control interaction, the model for this operational strategy necessarily comprises varying parameters depending on the considered operating point.

270 The resulting closed-loop power dynamics may be identified from data gained in simulations studies like discussed within this work. The employed model-based control approach briefly discussed, however, also inherently yields closed-loop model descriptions of the turbine by combining the controller and open-loop plant dynamics used in the design procedure, which are capable of portraying relevant dynamical aspects. The level of detail and identification of relevant dynamics of the turbine structure is not straightforward, where this contribution discussed some operational properties when considering the turbine as a variable power source.

275 *Code and data availability.* For inquiries about the source code and data, please reach out the corresponding author.

Author contributions. Florian Pöschke (FP) and Horst Schulte (HS) conceptualized the study and operating trajectories. FP conducted the control design and simulation studies. FP and HS analyzed the results, drew conclusions and created the manuscript.

Competing interests. The authors declare that they have no conflict of interest.

280 *Acknowledgements.* This project has received funding from the European Union's Horizon 2020 research and innovation programme under grant agreement No. 883985 (POSYTYF – POvering SYstem flexibiliTY in the Future through RES). <https://posytyf-h2020.eu/>



References

- Abouzeid, S. I., Guo, Y., and Zhang, H.-C.: Dynamic control strategy for the participation of variable speed wind turbine generators in primary frequency regulation, *Journal of Renewable and Sustainable Energy*, 11, 013 304, <https://doi.org/10.1063/1.5064846>, 2019.
- Aho, J., Fleming, P., and Pao, L. Y.: Active power control of wind turbines for ancillary services: A comparison of pitch and torque control methodologies, in: 2016 American Control Conference (ACC), pp. 1407–1412, <https://doi.org/10.1109/ACC.2016.7525114>, 2016.
- 285 Baerwald, E. F., Edworthy, J., Holder, M., and Barclay, R. M. R.: A large-scale mitigation experiment to reduce bat fatalities at wind energy facilities, *The Journal of Wildlife Management*, DOI: 10.2193/2008-233, 2009.
- Björk, J., Johansson, K. H., and Dörfler, F.: Dynamic Virtual Power Plant Design for Fast Frequency Reserves: Coordinating Hydro and Wind, 2021.
- 290 Bossanyi, E. A.: Wind turbine control for load reduction, *Wind Energy*, 6, <https://doi.org/10.1002/we.95>, 2003.
- Frederik, J. A., Weber, R., Cacciola, S., Campagnolo, F., Croce, A., Bottasso, C., and van Wingerden, J.-W.: Periodic dynamic induction control of wind farms: proving the potential in simulations and wind tunnel experiments, *Wind Energy Science*, 5, 245–257, <https://doi.org/10.5194/wes-5-245-2020>, 2020.
- Jain, A., Sakamuri, J. N., and Cutululis, N. A.: Grid-forming control strategies for black start by offshore wind power plants, *Wind Energy Science*, 5, 1297–1313, <https://doi.org/10.5194/wes-5-1297-2020>, 2020.
- 295 Jonkman, J. M. and Buhl, M. L.: FAST Users Guide, Tech. rep., National Renewable Energy Laboratory, 2005.
- Jonkman, J. M. and Buhl, M. L.: TurbSim User’s Guide, Tech. rep., National Renewable Energy Laboratory, 2006.
- Jonkman, J. M. and Jonkman, B. J.: FAST modularization framework for wind turbine simulation: full-system linearization, *Journal of Physics: Conference Series*, 753, 082 010, <https://doi.org/10.1088/1742-6596/753/8/082010>, 2016.
- 300 Jonkman, J. M., Butterfield, S., Musial, W., and Scott, G.: Definition of a 5-MW Reference Wind Turbine for Offshore System Development, Tech. rep., National Renewable Energy Laboratory, 2009.
- Kazda, J., Merz, K., Tande, J. O., and Cutululis, N. A.: Mitigating turbine mechanical loads using engineering model predictive wind farm controller, *Journal of Physics: Conference Series*, 1104, <https://doi.org/10.1088/1742-6596/1104/1/012036>, 2018.
- Kishor, N., Saini, R., and Singh, S.: A review on hydropower plant models and control, *Renewable and Sustainable Energy Reviews*, 11, 776–796, <https://doi.org/https://doi.org/10.1016/j.rser.2005.06.003>, 2007.
- 305 Leloudas, G., Zhu, W. J., Sørensen, J. N., Shen, W. Z., and Hjort, S.: Prediction and Reduction of Noise from a 2.3 MW Wind Turbine, *Journal of Physics: Conference Series*, 75, 012 083, <https://doi.org/10.1088/1742-6596/75/1/012083>, 2007.
- Machowski, J., Bialek, J., and Bumby, J.: *Power System Dynamics: Stability and Control*, John Wiley & Sons, Ltd, 2008.
- Margaris, I. D., Papathanassiou, S. A., Hatzigiorgiou, N. D., Hansen, A. D., and Sorensen, P.: Frequency Control in Autonomous Power Systems With High Wind Power Penetration, *IEEE Transactions on Sustainable Energy*, 3, 189–199, <https://doi.org/10.1109/TSTE.2011.2174660>, 2012.
- 310 Munters, W. and Meyers, J.: Towards practical dynamic induction control of wind farms: analysis of optimally controlled wind-farm boundary layers and sinusoidal induction control of first-row turbines, *Wind Energy Science*, 3, 409–425, <https://doi.org/10.5194/wes-3-409-2018>, 2018.
- 315 Petrović, V. and Bottasso, C. L.: Wind turbine envelope protection control over the full wind speed range, *Renewable Energy*, 111, 836 – 848, <https://doi.org/10.1016/j.renene.2017.04.021>, 2017.



- Pöschke, F., Gauterin, E., Kühn, M., Fortmann, J., and Schulte, H.: Load mitigation and power tracking capability for wind turbines using linear matrix inequality-based control design, *Wind Energy*, 23, 1792–1809, <https://doi.org/10.1002/we.2516>, 2020.
- 320 Rebelló, E., Watson, D., and Rodgers, M.: Ancillary services from wind turbines: automatic generation control (AGC) from a single Type 4 turbine, *Wind Energy Science*, 5, 225–236, <https://doi.org/10.5194/wes-5-225-2020>, 2020.
- Riboldi, C. E.: On the optimal tuning of individual pitch control for horizontal-axis wind turbines, *Wind Engineering*, 40, 398–416, <https://doi.org/10.1177/0309524X16651545>, 2016.
- Shan, M., Shan, W., Welck, F., and Duckwitz, D.: Design and laboratory test of black-start control mode for wind turbines, *Wind Energy*, 23, 763–778, <https://doi.org/10.1002/we.2457>, 2020.
- 325 Vali, M., Petrović, V., Steinfeld, G., Y. Pao, L., and Kühn, M.: An active power control approach for wake-induced load alleviation in a fully developed wind farm boundary layer, *Wind Energy Science*, 4, 139–161, <https://doi.org/10.5194/wes-4-139-2019>, 2019.
- Van de Vyver, J., De Kooning, J. D. M., Meersman, B., Vandeveld, L., and Vandoorn, T. L.: Droop Control as an Alternative Inertial Response Strategy for the Synthetic Inertia on Wind Turbines, *IEEE Transactions on Power Systems*, 31, 1129–1138, <https://doi.org/10.1109/TPWRS.2015.2417758>, 2016.
- 330 van Kuik, G. A. M., Peinke, J., Nijssen, R., Lekou, D., Mann, J., Sørensen, J. N., Ferreira, C., van Wingerden, J. W., Schlipf, D., Gebraad, P., Polinder, H., Abrahamsen, A., van Bussel, G. J. W., Sørensen, J. D., Tavner, P., Bottasso, C. L., Muskulus, M., Matha, D., Lindeboom, H. J., Degraer, S., Kramer, O., Lehnhoff, S., Sonnenschein, M., Sørensen, P. E., Künneke, R. W., Morthorst, P. E., and Skytte, K.: Long-term research challenges in wind energy – a research agenda by the European Academy of Wind Energy, *Wind Energy Science*, 1, 1–39, <https://doi.org/10.5194/wes-1-1-2016>, 2016.
- 335 Xin, H., Gan, D., Li, N., Li, H., and Dai, C.: Virtual power plant-based distributed control strategy for multiple distributed generators, *IET Control Theory & Applications*, 7, 90–98(8), <https://digital-library.theiet.org/content/journals/10.1049/iet-cta.2012.0141>, 2013.